Chemistry and Physics of Lipids 225 (2019) 104810

Contents lists available at ScienceDirect

Chemistry and Physics of Lipids

journal homepage: www.elsevier.com/locate/chemphyslip

Behaviour of protein (BSA)-lipid (DMPA) mixed monolayer on the spreading order of the individual component

Bijay K. Sah, Sarathi Kundu*

Soft Nano Laboratory, Physical Sciences Division, Institute of Advanced Study in Science and Technology, Vigyan Path, Paschim Boragaon, Garchuk, Guwahati, Assam 781035, India

ARTICLE INFO

Keywords:
BSA-DMPA mixed monolayer
Compression-decompression isotherm cycle
Hysteresis
Out-of-plane structures
Spreading order

ABSTRACT

Surface pressure (π) – mean molecular area (*A*) isotherms of protein (BSA) – lipid (DMPA) mixed films are examined by varying their ratio and altering the spreading order of BSA and DMPA on the water surface to study the protein-lipid interactions and the corresponding structures and patterns at different interfacial conditions. π–*A* isotherms and compression-decompression isotherm cycles of protein-lipid mixed monolayers below and above of the isoelectric point of BSA (pI ≈ 4.8) are also examined. Below the isoelectric point of BSA (pH ≈ 4.0), i.e., when BSA is weakly hydrophobic and has net positive charge shows low hysteresis irrespective of the spreading order of the molecules. However, at pH ≈ 7.0, i.e., when the overall charge of BSA is negative and is strongly hydrophobic the protein-lipid mixed films display higher hysteresis value. Besides the properties of the isotherms, the surface morphology and secondary conformations of protein inside the mixed films are obtained from X-ray reflectivity, atomic force microscopy (AFM) and Fourier transform infrared (FTIR) spectroscopy respectively after depositing the mixed films on solid substrates. Nearly similar information is obtained after altering the spreading order of BSA and DMPA, which indicates that the spreading of molecules on the water surface is one of the better ways of forming the lipid-protein mixed film at the air-water interface.

1. Introduction

In recent years, surface modifications and self-assembly of materials at interfaces have been studied intensively for the construction of different sensors (Stelzle et al., 1993; Sasaki et al., 1995), synthesis of novel organic and inorganic materials having ordered architecture in the nanoscale range (Peppas and Langer, 1994; Bunker et al., 1994; Douglas, 1996), targeted drug delivery (Laukkanen et al., 1994), catalysis (Mayor et al., 1996) and organisation of biological membrane (Grainger et al., 1992). Immobilization of biomaterials like proteins into a lipid membrane plays a vital role in mimicking the structures and functions of biological membranes. In general, protein adsorption at bio-interfaces has many biotechnological and biomedical applications (Castlden, 1969; Zhu et al., 1989; Okahata et al., 1989). Many proteins and lipids typically have the property to self-assemble at the interface to form organized structures or arrays (Whitesides and Boncheva, 2002). Protein-lipid two-component systems formed at the interfaces are effectively a combination of three interlinked interactions, i.e., protein-protein, lipid–lipid and lipid-protein interactions. Protein and lipid can interact in different ways like protein can get adsorb to hydrophilic headgroup or it may penetrate partially to the hydrophobic core of the bilayer membrane. In most of the cases, protein seems to be able to coordinate well with the hydrophilic as well as the hydrophobic regions of the membrane.

The interaction between the hydrophilic and hydrophobic parts of the lipid and protein plays an important role in determining the effective structure of the lipid-protein complex and the biological activities of the protein (Abney and Owicki, 1985). Behaviours of combined protein and lipid system are also dependent on the subphase pH, as according to the pH environment protein can alter the hydrophilic or hydrophobic exposure within a lipid layer (Sackmann, 1984). It has already been reported that alkalinity and acidity of the solvent plays a significant role in determining the surface hydrophobicity of the proteins like bovine serum albumin (BSA) (Alizadeh-Pasdar and Li-Chan, 2000). It exhibits lower surface hydrophobicity in a stronger acidic media (pH ≈ 3.0–4.0) in comparison to the neutral (pH ≈ 7.0) or basic (pH ≈ 9.0) media (Alizadeh-Pasdar and Li-Chan, 2000). Moreover, in presence of negatively charged DMPA monolayer the surface pH becomes lower than the subphase pH (Gaines, 1966). As a result, structural modifications in the lipid-protein complexes occur, which have effects on their thermodynamic, mechanical and conformational properties (Jahnig et al., 1982).

* Corresponding author.
E-mail address: sarathi.kundu@gmail.com (S. Kundu).

https://doi.org/10.1016/j.chemphyslip.2019.104810
Received 30 April 2019; Received in revised form 24 July 2019; Accepted 10 August 2019
Available online 12 August 2019
0009-3084/

Langmuir monolayer of phospholipid is considered as a model membrane formed at the air-water interface (Caetano et al., 2001; de Souza et al., 2006; Vernoux et al., 2007; Wang et al., 2004). Studies on Langmuir monolayers have several advantages since allow to fix, among others surface parameters the surface composition, molecular arrangement, lateral packing or surface pressure and physical state of the lipid phase. Besides, the conditions can also be tuned by changing some parameters in the subphase like subphase pH, dissolved specifically ions and molecules, ionic strength and/or temperature. Usually, to form a mixed monolayer at the air-water interface, the most convenient way is to dissolve the component molecules inside a suitable common solvent and then spread over the water surface. However, in forming protein and lipid mixture there is no any common solvent of single component although specific multi-component solvent was used in forming such mixture (Fidelio et al., 1984). As a consequence, most works on lipid-protein mixed monolayer are carried out either by injecting the protein into the water subphase on a previously covered lipid monolayer (Wang et al., 2001) or by dissolving a suitable amount of protein in the water subphase and then spreading the lipid molecules on water surface to form a mixed monolayer at the air-water interface (Zhang et al., 2000; Li et al., 1998; Wang et al., 2002). However, in the processes mentioned above, it becomes challenging to estimate the number of protein molecules participating in the interaction with the lipids. In order to estimate the number of molecules participating in the interaction, both proteins and lipids are required to spread on the water surface from their solutions of known concentrations to form a protein-lipid mixed monolayer. However, in that proposed method, monolayer properties, related structures and patterns may vary depending upon the spreading order of the protein and lipid for a particular surface pH.

In this article, we have studied on the lipid-protein mixed films using phospholipid DMPA (1, 2-dimyristoyl-*sn*-glycero-3-phosphate), which possess a single negative charge (Martin et al., 1996) and globular protein BSA (bovine serum albumin) having an oblate ellipsoid shape of dimensions ≈9 Å × 42 Å × 42 Å (Sah and Kundu, 2017) and have net positive or negative surface charges depending upon the subphase pH. It is found that BSA is a soft protein molecule without having a high degree of structural stability (Peters, 1985) that often results in conformational changes during adsorption (Norde and Favier, 1992; Kondo et al., 1991; Giacomelli and Norde, 2001). However, it shows unaltered structure from pH ≈ 4.0 to ≈9.0 within the concentration range of 10–50 mg/ml (Kundu et al., 2013) and therefore two different pH values (≈4.0 and 7.0), i.e., below and above the isoelectric point of BSA (pI ≈ 4.8) are chosen for our study. Pure lipid or mixture of lipid-protein monolayer shows different thermodynamic phases and phase transitions under different physiochemical conditions like pH, dissolve ions, temperature (Garcia-Manyes et al., 2006; Cremer and Boxer, 1999; Reimhult et al., 2003; Keller and Kasemo, 1998; McConnell and Moy, 1988; McConnell and De Koker, 1992; Lösche and Mohwaid, 1984). Here, we have tried to explore the phases of the protein-lipid (BSA-DMPA) and lipid-protein (DMPA-BSA) mixed monolayer above and below the isoelectric point of BSA at the air-water interface along with their structure and morphology obtained from the films deposited on solid surfaces. Besides, we have also identified the modifications occurring in the π–A isotherms and stability behaviours of mixed monolayers due to the change in the ratio of the constituent protein and lipid molecules. The compression-expansion isotherm cycles of BSA-DMPA and DMPA-BSA mixed monolayers are also taken at both pH ≈ 4.0 and ≈7.0. A comparative study on the hysteresis and compressibility (κ) are obtained from the compression-expansion cycles and surface pressure - mean molecular area (π-A) isotherms. After depositing the mixed monolayers on Si (001) substrates, atomic force microscopy (AFM) is used to acquire the surface morphologies of the films. X-ray reflectivity (XRR) and Fourier transform infrared (FTIR) spectroscopy is used to get the out-of-plane structures and secondary conformations of protein inside the protein-lipid and lipid-protein mixed monolayers at different physiochemical conditions.

2. Experimental

Bovine Serum Albumin (BSA) (catalog No. A2153) and phospholipid DMPA (catalog No. 830845P) was purchased from Sigma-Aldrich and Avanti polar lipids respectively. BSA is used as purchased without any further purification so it is not free from essential fatty acids. The stock solution of BSA of concentration 1 mg/ml was prepared using Milli-Q water (resistivity ≈ 18.2 MΩ cm) and DMPA solution of concentration 0.5 mg/ml was prepared in chloroform. DMPA is a well-studied lipid molecule and the structures, phase behaviours and domain patterns of DMPA monolayer phases are already reported by other groups (Lösche and Mohwaid, 1984; Vaknin et al., 2003; Schalke et al., 2000). Like other lipids, the headgroups of DMPA lipid are of particular interest as such negatively charged headgroups are treated as interaction sites with the aqueous environment and also with the ions and charged molecules like proteins. On the other hand, globular proteins such as BSA even after being water soluble can form stable monolayer at the air-water interface. Such protein films at the air-water interface can be formed by spreading the desired amount of protein solution on the water surface (Sah and Kundu, 2017; Tronin et al., 1994). Moreover, as the isoelectric point (pI) of BSA is ≈4.8, therefore, the net surface charge of such protein molecules can be tuned from positive to negative values by changing the subphase pH from ≈4.0 to 7.0, and accordingly the lipid-protein interaction may be varied. BSA protein and DMPA lipid were spread carefully one after the other with a syringe on the water surface in a Langmuir trough (Apex Instruments) keeping a time gap of 15 min to form BSA-DMPA mixed monolayer. Similarly, by reversing the order of spreading molecules and keeping all the other parameters same, DMPA-BSA mixed monolayer was also formed. Any change in the surface tension was recorded through a Wilhelmy plate which is connected to an electro-balance. Compression and expansion of the monolayers for isotherm and hysteresis measurements were carried out at a constant barrier speed of 5 mm/min. Before the deposition, time lapse of about 15 min was allowed to gain stability of the film. All the Langmuir-Blodgett (LB) depositions were performed using the dipping speed of 2 mm/min. Before deposition, Si (001) substrates were made hydrophilic after placing them in a mixed solution of ammonium hydroxide (NH_4OH, Merck, 30%), hydrogen peroxide (H_2O_2, Merck, 30%), and Milli-Q water (H_2O: NH_4OH: H_2O_2 :: 2:1:1, by volume) for 5–10 min at 100 °C. The substrates were immersed into Milli-Q water as soon as the cleaning is over, until being used in LB deposition. All π-A isotherm measurements and film depositions were performed at room temperature (≈ 23 °C). The pH of the water subphase was kept constant at ≈4.0 (using HCl) and 7.0 (using NaOH) for different experimental conditions. The use of buffer was avoided to minimize the contamination.

Surface topography of the mixed films deposited by LB technique at different subphase pH was studied through Atomic Force Microscope (NTEGRA Prima, NT-MDT Technology). Semi-contact mode was used for all the scans using silicon cantilever having spring constant of ≈11.8 N/m (Das et al., 2017). All the scans were carried out in a constant force mode over different portions of the films with a scan area of 3 μm × 3 μm. WSxM software (Horcas et al., 2007) was used for AFM image processing and analysis. The attenuated total reflection–Fourier transform infrared (ATR-FTIR) spectroscopy was also performed over the mixed films. Data were taken using spectrophotometer NICOLET 6700 (Thermo- Fisher) within the wavelength range of 380–4000 cm^{-1} at 4 cm^{-1} resolution.

All DMPA-BSA and BSA-DMPA mixed thin films were also examined by X-ray reflectivity (XRR) measurements using an X-ray diffractometer setup. Diffractometer (D8 Advanced, Bruker AXS) has a copper (Cu) source in a sealed tube followed by a Göbel mirror for the selection and enhancement of the Cu K_α radiation (=1.54 Å). The scattered beam was detected using NaI scintillation (point) detector. The data were taken in a specular condition, i.e., the incident and reflected angle (θ) was kept the same, and both lie in the same scattering plane. Under

these conditions, there exists a non-vanishing wave vector component $q_z = \frac{4\pi}{\lambda}\sin\theta$. XRR data analysis was pursued using Parratt's formalism (Parratt, 1954), where the film is assumed to have a stack of multiple homogeneous layers having sharp interfaces. Surface and interfacial roughnesses were also included in order to analyze the XRR data (Daillant and Gibaud, 2009; Tolan, 1999). Electron-density profile (EDP) is extracted from the data fitting (Daillant and Gibaud, 2009; Basu and Sanyal, 2002), which gives in-plane (x–y) average electron density (ρ) as a function of depth (z) with high resolution (Daillant and Gibaud, 2009; Tolan, 1999; Basu and Sanyal, 2002; Kundu et al., 2006; Kundu et al., 2005).

3. Results and discussion

Phase transitions and different phases of the monolayers at the air-water interface can be interpreted from π–A isotherms. Here, A represents the average area occupied by all the BSA and DMPA molecules at the air-water interface. The molecular weight of BSA and DMPA mixture was calculated using the formula

$$M = \frac{m_1 c_1 v_1 + m_2 c_2 v_2}{c_1 v_1 + c_2 v_2} \quad (1)$$

where c_1, c_2, m_1, m_2, v_1, and v_2 are the concentration, molecular weight and volume of BSA and DMPA respectively. The interactions among the molecules in the monolayer lead to different phase transitions as identified from the changes in the π–A isotherms. Fig. 1(a)–(d) show the π-A isotherms of mixed monolayers for different volume ratios of BSA and DMPA at pH below and above (pH ≈ 4.0 and 7.0) the isoelectric point (pI ≈ 4.8) of BSA. Isotherms at pH ≈ 4.0 for different ratios of BSA and DMPA in the mixed film are shown in Fig. 1(a), where BSA is spread before DMPA (this condition will be further referred as B/D throughout the article) after a time gap of 15 min. Cases where DMPA is spread before BSA are referred as D/B. Different color codes are used to distinguish different BSA:DMPA ratios: red (150:0), blue (120:30), dark yellow (90:60), cyan (75:75), magenta (30:120) and orange (0:150). For the corresponding mixed monolayers the amount of protein present in terms of mole fractions (X_p) are 1.0, 68.7×10^{-3}, 27.9×10^{-3}, 17.7×10^{-3}, 4.1×10^{-3} and 0.0 respectively. The corresponding protein coverage values in the mixed films are 100.0%, 89.5%, 77.5%, 68.4%, 33.1% and 0.0% respectively. For different BSA:DMPA ratios, π starts to increase from different mean molecular area (A_0) ≈ 92 (B1/D1), 88 (B2/D2), 80 (B3/D3), 64 (B4/D4), 51 (B5/D5) and 0.51 (B6/D6) nm^2 respectively. The decrease in BSA's proportion or increase in DMPA's proportion in the ratio results in the decrease in A_0 value. In addition to that, it is also seen that the monolayer (from B3/D3 to B6/D6) achieves higher surface pressure ≈40 mN/m, but the surface pressure achieved by B1/D1 and B2/D2 is ≈20 mN/m. Fig. 1(b), on the other hand, shows the π-A isotherms for the films where DMPA is spread before the BSA (D/B) at same pH ≈ 4.0. The area per molecule obtained against the rise in surface pressure for different isotherms are

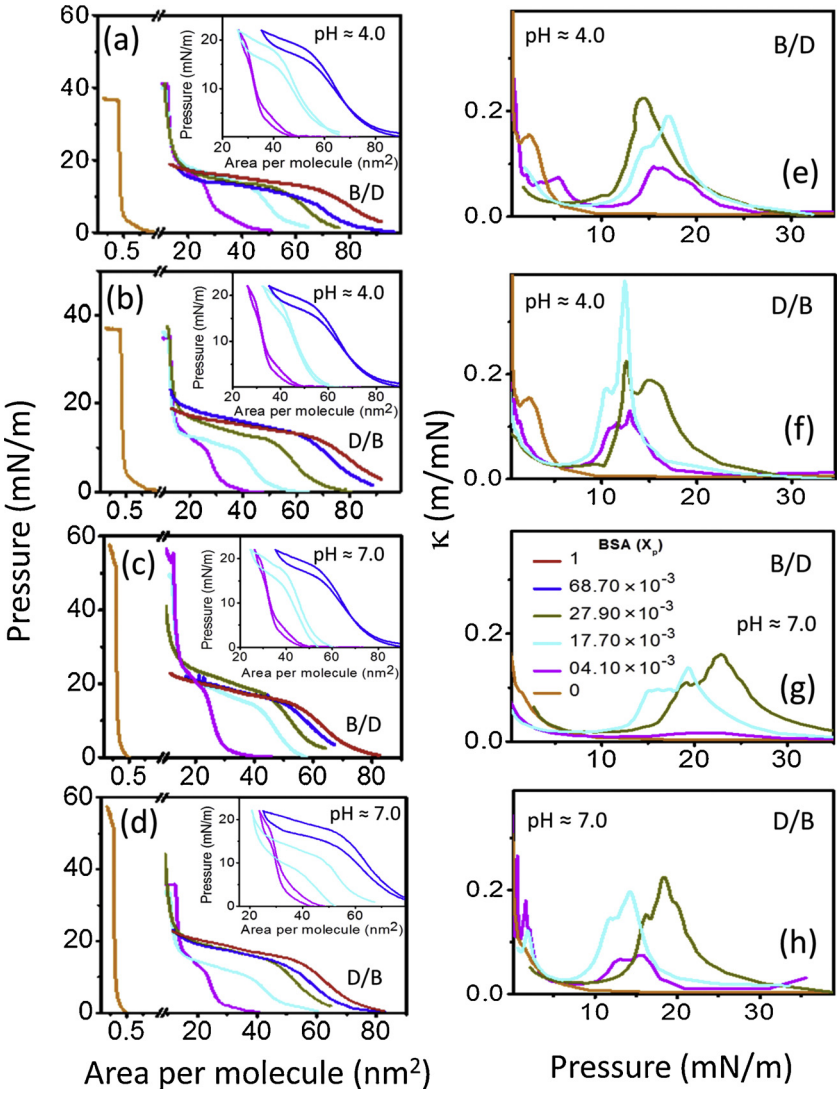

Fig. 1. Left Column: Surface pressure - mean molecular area (π-A) isotherms of BSA-DMPA mixed monolayer at two different subphase pH values, i.e., at pH ≈ 4.0 (a–b) where figure (a) depicts B/D combinational order whereas figure (b) shows D/B order, and at pH ≈ 7.0 where figure (c) and (d) stands for B/D and D/B combinational order respectively. Six colours represent six different ratios of BSA:DMPA mixed films: red (150:0), blue (120:30), dark yellow (90:60), cyan (75:75), magenta (30:120), orange (0:150). The corresponding BSA mole fractions (X_p) are 1.0, 68.7×10^{-3}, 27.9×10^{-3}, 17.7×10^{-3}, 4.1×10^{-3} and 0.0 respectively. Inset: corresponding compression-decompression isotherm cycles of mixed films. Right Column (e–h) shows variation of isothermal compressibility (κ) with monolayer surface pressure (π) corresponding to their left counterparts of π-A isotherms.

$A_0 \approx 92$ (D1/B1), 88 (D2/B2), 80 (D3/B3), 57 (D4/B4), 40 (D5/B5) and 0.51 (D6/B6) nm^2 respectively. Similarly, Fig. 1(c) and (d) shows the same set of six π-A isotherms but at pH ≈ 7.0. Fig. 1(c) shows that the surface pressure starts to rise from $A_0 \approx 82$ (B1/D1), 69 (B2/D2), 64 (B3/D3), 58 (B4/D4), 37 (B5/D5) and 0.57 (B6/D6) nm^2, whereas, Fig. 1(d) shows the rise in π from $A_0 \approx 82$ (D1/B1), 76 (D2/B2), 65 (D3/B3), 60 (D4/B4), 40 (D5/B5) and 0.57 (D6/B6) nm^2 respectively. Corresponding insets in Fig. 1(a)–(d) show the compression-decompression π-A isotherms for three different volume ratios of BSA:DMPA, i.e., for 120:30 (blue), 75:75 (cyan) and 30:120 (magenta) of BSA:DMPA for different pH and spreading conditions. It is reported before that the first discontinuity or bending in the π-A isotherm occurs at ≈13–15 mN/m ($A \approx 60\ nm^2$)for pH ≈ 5.0–6.0 (Muramatsu and Sobotka, 1962; Fidelio et al., 1984). In our study, such bending is observed nearly at the same pressure in the π-A isotherms and it occurs at $A \approx 70$ and 60 nm^2 for pH ≈ 4.0 and 7.0 respectively. It is also observed that for higher lipid/protein ratio and when lipid is spread first the bending or exclusion plateau of the protein occurs at $\pi \approx 15$ mN/m, which is relatively less than the plateau pressure of ≈20 mN/m as obtained for all other spreading conditions for both the pHs. Probably, when the lipid is spread former to the protein and the amount of lipid is more in the respective mixtures then the lipid behavior in the mixed film dominates the overall nature of the isotherm and as a result the BSA plateau occurs at relatively lower pressure, i.e. at $\pi \approx 15$ mN/m. For every compression-decompression cycle, a certain amount of hysteresis exists, and it has been tabulated in Table 1. From the hysteresis values displayed in Table 1 it is evident that in all the cases irrespective of any ratios and spreading order, hysteresis is less at pH ≈ 4.0 in comparison to pH ≈ 7.0.

Isothermal compressibility (κ), where $\kappa = -1/A(\partial A/\partial \pi)_T$ (Chou and Chang, 2000), of the monolayer mixture are calculated for (B3/D3), (B4/D4), (B5/D5) and (B6/D6) for both the pH conditions. κ values are also calculated for (D3/B3), (D4/B4), (D5/B5) and (D6/B6) for both the pH conditions. For the ratios of (B1/D1 and D1/B1) and (B2/D2 and D2/B2) the isothermal compressibility curves are avoided as they could not achieve higher surface pressure in the π-A isotherms. Fig. 1(e) and (f) show the κ vs. π plot for pH ≈ 4.0 and Fig. 1(g) and (h) show the same for pH ≈ 7.0. The color codes are kept same as that of the π-A isotherms for better understanding. From the compressibility curves shown in Fig. 1(e)–(h), it is evident that the mixed monolayer transforms from one less compressible phase to another less compressible phase through a relatively higher compressible phase. However, among the two less compressible phases (corresponding κ values are ≈0.031 and ≈0.011 m/mN) the compressibility is relatively higher for the first phase, i.e., the phase that obtained at lower surface pressure. It is also observed that for both the spreading conditions (B/D and D/B), relatively higher compressible phase is present for the intermediate ratios, i.e., for 90:60 (dark yellow), 75:75 (cyan), 30:120 (magenta). The less compressible solid phase was also obtained from the mixed monolayers for the same intermediate ratios.

Mixed monolayers for which compression was performed up to higher surface pressure ($\pi \approx 32$ mN/m) show a significant increase in the hysteresis area, as shown in Fig. 2. The π-A isotherm cycles for higher pressure are carried out only for equal volume ratio of DMPA and BSA, i.e., for 75:75 (B4/D4 and D4/B4) or $X_p : X_l = 17.70 \times 10^{-3} : 98.23 \times 10^{-2}$. The last row of Table 1 summarizes the hysteresis values obtained from the isotherm cycles performed up to $\pi \approx 32$ mN/m. Fig. 2(a) and (b) show the π-A isotherm cycles both at pH ≈ 4.0 (green) and 7.0 (purple) for B/D and D/B films respectively. The insets illustrate the corresponding isotherm cycles for the lower surface pressure (22 mN/m). The consecutive two π-A isotherm cycles at pH ≈ 4.0 and 7.0 in the B/D conditions are also shown in Fig. 2(c) and (d) respectively. The solid line is used for the first cycle whereas the dashed line is used for the second cycle. It is observed that for both the pH conditions the overall nature of the isotherm cycles remain nearly same except some minute variations as the area per molecule is little less for both the raising and target surface pressures during second compression. However, such decrement in area per molecule during second compression can occur due to two reasons: defects or voids may get reduced due to the effect of first compression and BSA molecules may shift toward the hydrophobic tail region/air-side of lipid. Although the loss of materials from the film may also cause such lower molecular area but that possibility is ruled out as pure BSA shows reversible hysteresis as is discussed in the next section.

Being a water-soluble protein, BSA may get desorbed into the water subphase from the films formed at the air-water interface. To observe the desorption process of BSA molecules into the water subphase, compression-decompression π-A isotherms are performed. Fig. 3(a) shows the π-A isotherm cycles for pure BSA monolayer at pH ≈ 4.0 (red) and 7.0 (blue). At pH ≈ 4.0, π starts to rise when the area per molecule, i.e., A_0 is ≈93 nm^2 whereas for pH ≈ 7.0 the same is observed at ≈80 nm^2. It is also found that the decompression curve converges with the compression curve for both the pH conditions at zero surface pressure. It thus indicates that even after being water-soluble protein, the loss of BSA molecule into the water subphase is negligible. The stability of the monolayers at the air-water interface can be estimated from the area relaxation curves at constant surface pressure (Stallberg-Stenhagen and Stenhagen, 1945). The stability of the pure and mixed films are studied from the A-t curves, which are shown in Fig. 3(b) and (c) respectively. For all the A-t measurements, the films are allowed an equilibrium time of 15 min after the spreading of the molecules. Fig. 3(b) shows the A-t curves for pure DMPA (orange) and pure BSA (red) films for both the lower and higher constant target pressures (π_T) at pH ≈ 7.0. The corresponding inset illustrates the stability curves for both pure DMPA (orange) and BSA (red) at pH ≈ 4.0. For pure DMPA monolayers, the area relaxation curves show very stable film for both the lower (≈22 mN/m) and higher (≈32 mN/m) π_T. However, for pure BSA monolayers, lower π_T (≈11 mN/m) shows a more stable film compared to higher π_T (≈22 mN/m). Stability of BSA film is decreased at higher surface pressure because the BSA molecules might have transferred to the air side of the air-water interface at higher π_T forming a bilayer like structure (Sah and Kundu, 2017). In Fig. 3(c), stability curves (i.e., A-t curves) for both the pH conditions (≈4.0 and 7.0) and also for the lower and higher constant surface pressures (22 and 32 mN/m) are shown for equal BSA and DMPA volume ratio, i.e., for B4/D4 and D4/B4. Actually, the A-t curves for the pH ≈ 4.0 are shown in the inset of the corresponding figure. Unlike pure BSA, the mixed film shows more stability at $\pi_T \approx 32$ mN/m compared to the

Table 1
Hysteresis values obtained from the compression-decompression isotherm cycles for different ratios at two different pH (≈4.0 and 7.0) values and two different spreading conditions.

Mixing Ratio		pH ≈ 4.0		pH ≈ 7.0	
BSA (X_p)	DMPA (X_l)	B/D	D/B	B/D	D/B
4.10×10^{-3}	99.59×10^{-2}	28.23×10^{-21} N m	28.72×10^{-21} N m	66.20×10^{-21} N m	45.11×10^{-21} N m
17.70×10^{-3}	98.23×10^{-2}	49.03×10^{-21} N m	33.14×10^{-21} N m	69.67×10^{-21} N m	154.82×10^{-21} N m
68.70×10^{-3}	93.13×10^{-2}	35.86×10^{-21} N m	35.74×10^{-21} N m	161.24×10^{-21} N m	130.61×10^{-21} N m
17.70×10^{-3} (high π)	98.23×10^{-2} (high π)	182.35×10^{-21} N m	233.11×10^{-21} N m	194.17×10^{-21} N m	242.16×10^{-21} N m

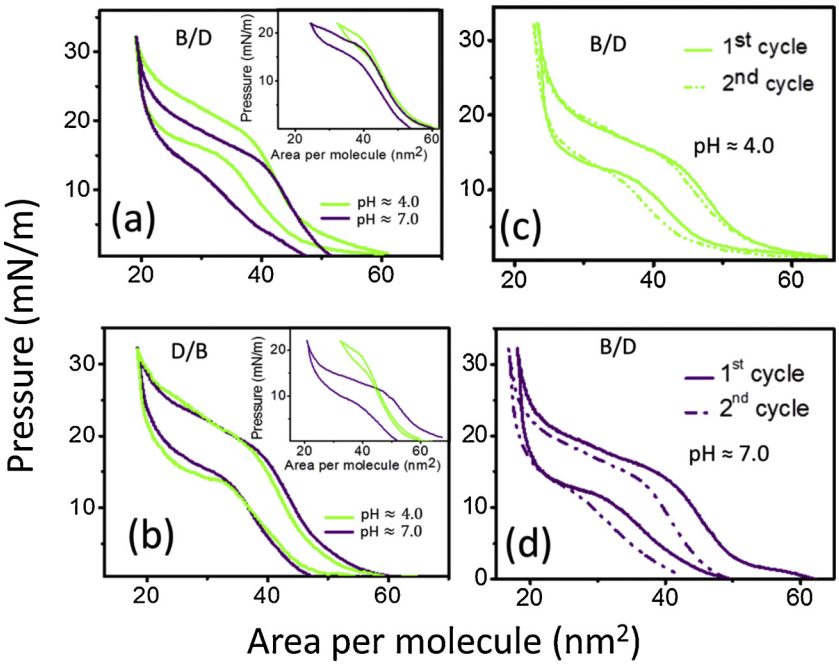

Fig. 2. Compression-decompression isotherm cycles of BSA and DMPA mixture (a) B/D and (b) D/B films at pH ≈ 4.0 (green) and 7.0 (purple) at higher surface pressure (32 mN/m). The insets illustrate the corresponding isotherm cycles for lower surface pressure (22 mN/m). The consecutive two cycles of π-*A* isotherm in the B/D condition is shown for pH ≈ 4.0 (c) and 7.0 (d) respectively.

$\pi_T \approx 22$ mN/m for both the spreading and pH conditions. For mixed films at higher constant pressure ($\pi_T \approx 32$ mN/m), BSA molecules might have transferred to the hydrobhobic tail region of the lipid molecules during monolayer compression up to $\pi_T \approx 32$ mN/m and therefore with time further transfer toward the tail region/air-side was negligible. BSA molecules placed in the hydrophobic tail regions of lipid molecules is also evidensed from the XRR analysis and the corresponding results are discussed in the following section. Fig. 3(d) shows the *A-t* curves for mixed BSA and DMPA film (B/D) for different BSA:DMPA volume ratios at pH ≈ 7.0 and $\pi_T \approx 22$ mN/m. The color code is same as that of Fig. 1. The arrow indicates the direction of increasing BSA ratio in the mixed film. Stability of the mixed film gradually decreases with the increasing BSA ratio in the film. Thus, at $\pi_T \approx 22$ mN/m, transferring of BSA molecules toward the hydrophobic tail region/air-side of lipid is possible with time as the monolayer compression was limited within 22 mN/m and as a result more transfer occurs for which more BSA molecules exist in the film. Similar results were obtained for pH ≈ 4.0, so it is not shown here.

To study the structures and surface morphology of the mixed films, equal volume ratios (75:75) of BSA and DMPA mixtures were deposited on hydrophilic silicon Si (001) substrates in a single upstroke for both the B/D and D/B conditions at different points of the isotherms. AFM images depicting the surface topography of BSA and DMPA mixed films for equal volume ratios (75:75) are shown in Fig. 4, where the first and second column represents the films deposited at lower (π = 10 mN/m) and higher (π = 40 mN/m) surface pressure during first compression, while the third column represents the films deposited at same lower pressure (π = 10 mN/m) during the second compression for two different subphase pH ≈ 4.0 (Fig. 4(a)–(f)) and 7.0 (Fig. 4(g)–(l)) respectively. First and third row corresponds to B/D whereas second and fourth row corresponds to D/B. Irrespective of B/D and D/B conditions, the films show firmly smooth morphology for the lower pressure during both the compression (first and second) whereas for the higher pressure in some cases small globule-like structure is more pronounced. Height profiles obtained from the images show variation in heights from 0.3 to 0.8 nm for lower pressure under first and second compression, on the

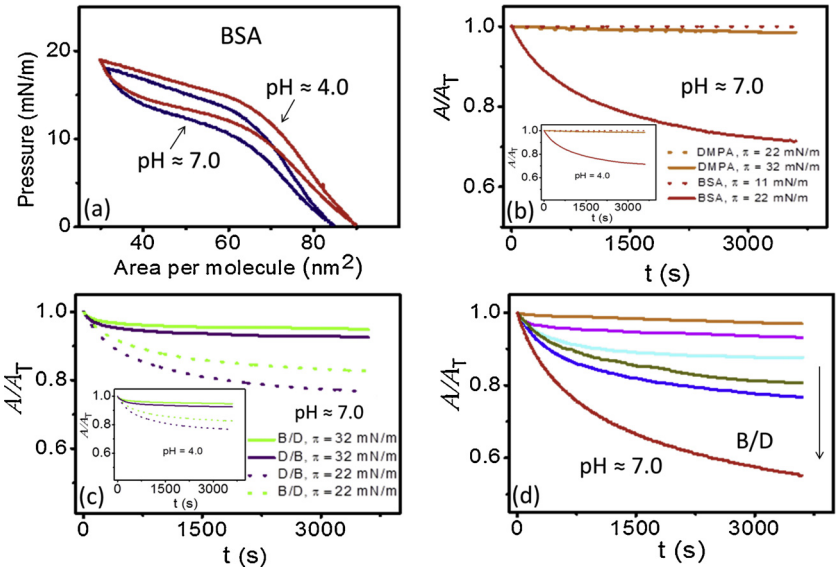

Fig. 3. (a) Compression-decompression isotherm cycles of BSA at pH ≈ 4.0 (red) and ≈7.0 (blue) respectively. (b) Stability curves (*A-t*) of the pure BSA, DMPA and mixed films (c) at lower (22 mN/m) and higher (32 mN/m) constant target pressures (π_T) at pH ≈ 7.0. The insets show the same at pH ≈ 4.0. (d) Stability for different ratios of BSA:DMPA mixed films are shown at pH ≈ 7.0. Colours indicates the respective ratios of BSA:DMPA mixed films: red (150:0), blue (120:30), dark yellow (90:60), cyan (75:75), magenta (30:120) and orange (0:150), i.e., the corresponding BSA mole fractions (X_p) are 1.0, 68.7×10^{-3}, 27.9×10^{-3}, 17.7×10^{-3}, 4.1×10^{-3} and 0.0 respectively.

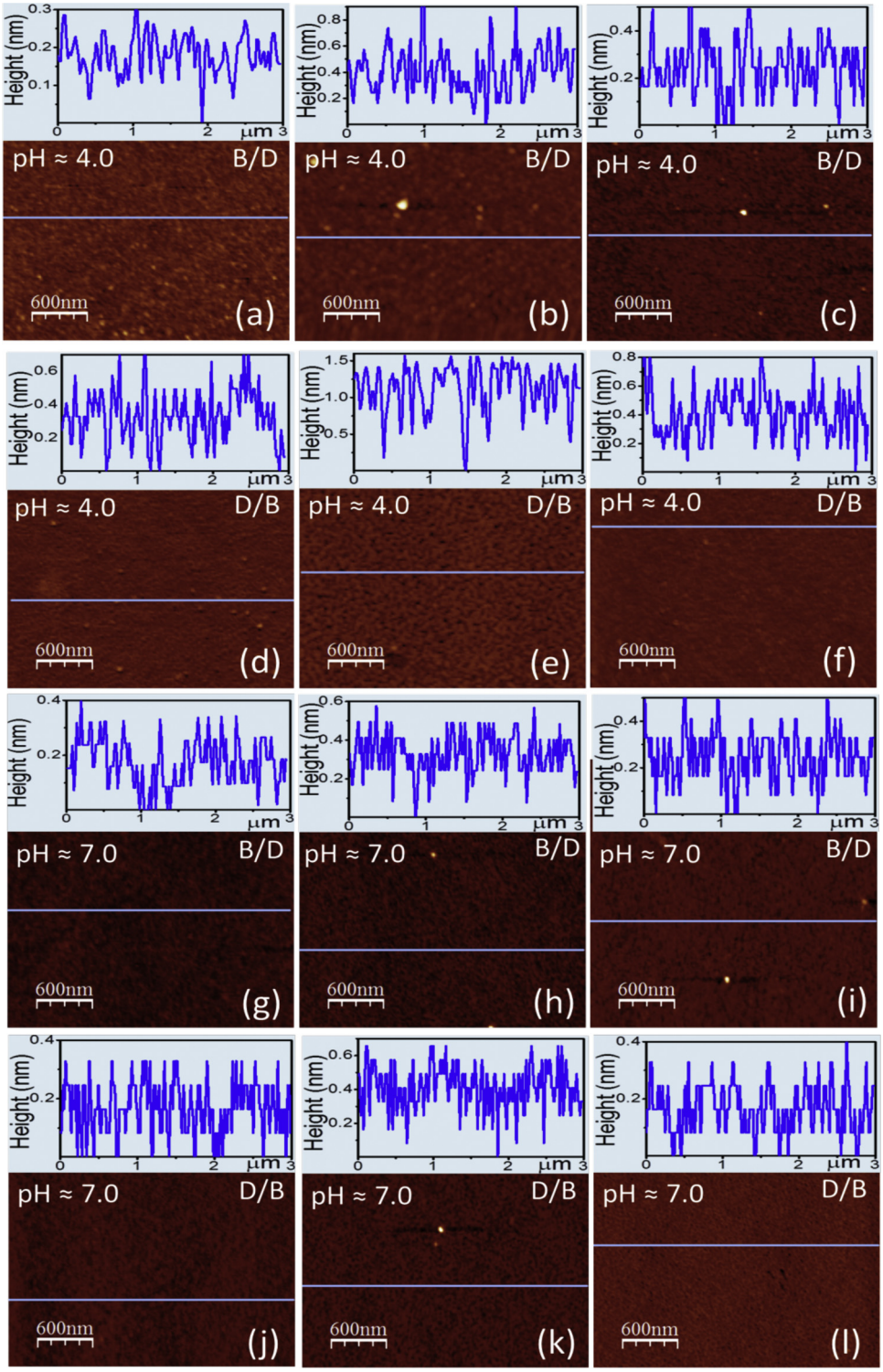

Fig. 4. AFM images of BSA and DMPA mixed films deposited on Si (001). First and second column are for the films deposited at lower (π = 10 mN/m) and higher (π = 40 mN/m) surface pressure during first compression, while third column is for the films deposited at lower pressure (π = 10 mN/m) during the second compression at two different pH values ≈4.0 (a–f) and 7.0 (g–l). First and third row for the BSA-DMPA films, whereas second and fourth row for DMPA-BSA films. Scan size: 3 μm × 3 μm. Insets are the corresponding line profiles. The bars represent 600 nm.

other hand, for higher pressure the line profiles varied from 0.7 to 1.5 nm.

Conformations of protein inside protein-lipid mixed films are identified from ATR-FTIR peaks present in the Amide-I band (1700–1600 cm^{-1}) as it is considered as the most sensitive spectral region for obtaining information of secondary structures of proteins (Kong and Yu, 2007). Within Amide-I band, a total of 14 peaks were obtained as shown in Fig. 5. All the designated peaks are assigned according to the literature showing different secondary structures such as beta sheet, beta-turn, anti-parallel beta sheet, alpha helix, intra- and inter-molecular beta strand, random coil (Kong and Yu, 2007; Murayama and Tomida, 2004). From Fig. 5 it is observed that the peaks

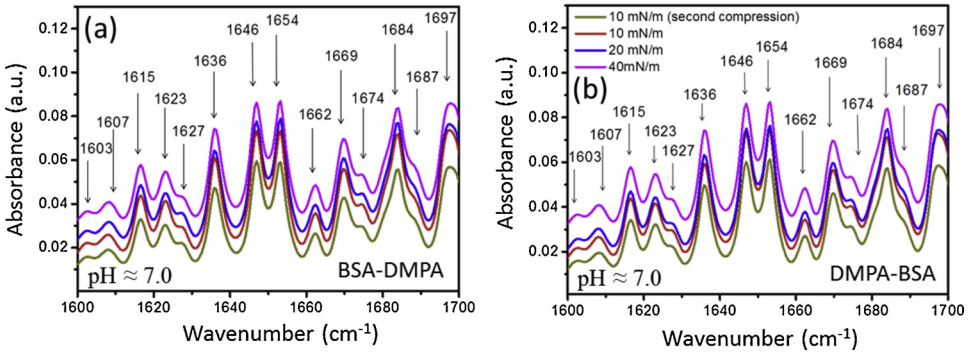

Fig. 5. ATR-FTIR spectra of Amide-I region obtained from (a) BSA-DMPA and (b) DMPA-BSA mixed films at pH ≈ 7.0 for different pressure conditions, i.e., during first compression at pressure 10 mN/m (red), 20 mN/m (blue), 40 mN/m (magenta) and again at 10 mN/m (dark yellow) during second compression. Arrows indicate the corresponding peak positions.

found at 1623, 1627, 1636 and 1697 cm^{-1} are related with the beta sheet and the peaks obtained at 1669, 1674, 1684 and 1687 cm^{-1} are related to beta-turn. Other peaks observed at 1603, 1607, 1615, 1646, 1654 and 1662 cm^{-1} correspond to side chain vibration, intermolecular beta strand, intramolecular beta strand, random coil, alpha helix, and 3_{10} helix respectively. For all the surface pressure conditions, the peak positions remain nearly unaltered indicating that the BSA and DMPA mixed films preserve all the secondary structures of the protein; however, slight changes in the peak intensity implies the possibility of some conformational changes during the compression process. Data obtained from ATR-FTIR show similar peaks for both the spreading conditions and at both the subphase pH (≈4.0 and 7.0) values. The ATR-FTIR results obtained for pH ≈ 4.0 is not shown here as it is nearly similar to the results obtained for pH ≈ 7.0.

X-ray reflectivity data (open circles) and the corresponding fitted lines at pH ≈ 4.0 and 7.0 for B/D condition are shown in Fig. 6(a) and (c), whereas the EDPs are shown in Fig. 6(b) and (d) respectively. EDPs obtained from the BSA-DMPA films deposited at π ≈ 10 mN/m, i.e., at lower surface pressure indicate that monolayer structure is present for both the pH values. However, for the films deposited at higher surface pressure, i.e., at π ≈ 40 mN/m, EDPs show a modest increase in electron density and thickness, indicating that some BSA molecules might have driven slightly towards the lipid hydrophobic tail part or air-side from the air-water interface. The shifting of the BSA molecules is evidenced by the EDPs shown in Fig. 6(b) and (d) as relatively higher electron densities (≈0.70 and 0.92 el/Å^3) are obtained at ≈27 Å from the substrate surface in addition with the relatively higher electron densities (≈0.86 and 1.12 el/Å^3) near the substrate surface for pH ≈ 4.0 and 7.0 respectively, which is responsible for both the lipid headgroups and BSA. From the films deposited during second compression at π ≈ 10 mN/m, EDPs indicate that nearly the initial state of the monolayer is achieved with minute variations in comparison with the first compression at similar pressure for pH ≈ 4.0. However, for pH ≈ 7.0 although nearly the same thickness is found as it was obtained during the first compression, but electron density is relatively increased. This suggests that the molecules once lifted from the air-water interfaces finds difficulty in coming back fully to its initial state, which was not the case when the subphase pH was ≈4.0. This observation is found to be well in agreement with the results obtained from the π-*A* isotherm cycles, as mostly irreversible hysteresis are observed for pH ≈ 7.0, while nearly reversible hysteresis for pH ≈ 4.0. X-ray reflectivity data (open circles) and the corresponding fitted lines at pH ≈ 4.0 and 7.0 for D/B condition, i.e., for DMPA-BSA films are shown in Fig. 7(a) and (c), whereas the EDPs are shown in Fig. 7(b) and (d) respectively. EDPs obtained from the DMPA-BSA films deposited at π ≈ 10 mN/m clearly indicate that like B/D condition, monolayer

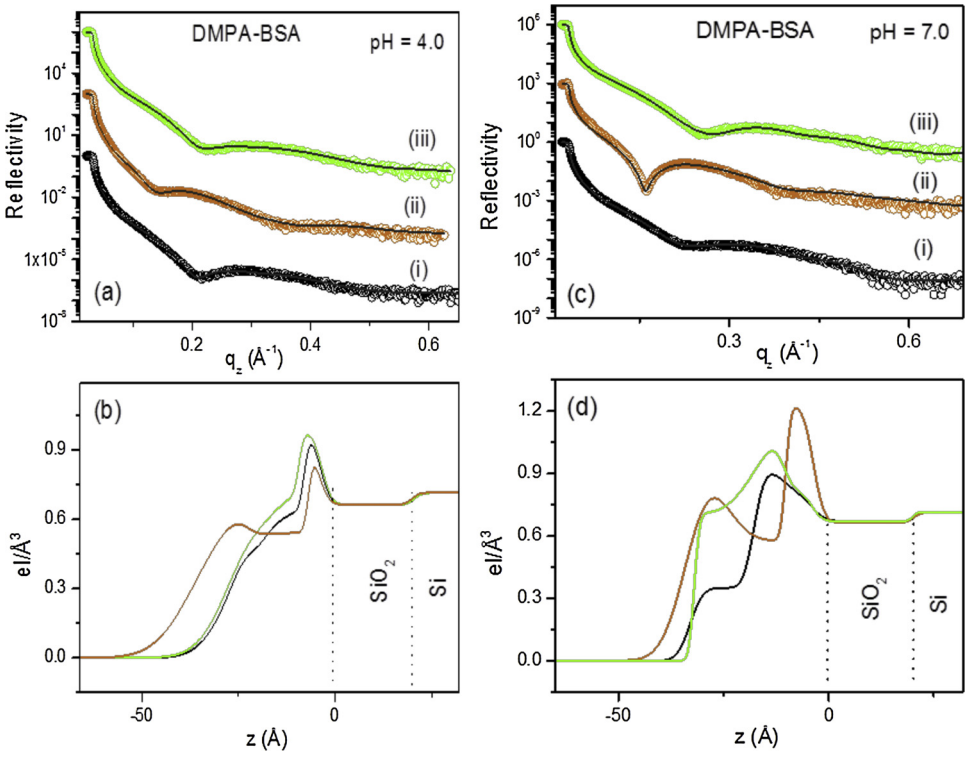

Fig. 6. X-ray reflectivity data (circle) and the corresponding fitted curves (solid line) obtained from the DMPA-BSA mixed films at (i) 10 mN/m and (ii) 40 mN/m during first compression, and again at (iii) 10 mN/m during second compression at (a) pH ≈ 4.0 and (c) pH ≈ 7.0. (b) and (d): corresponding electron density profiles extracted from the fitting of the reflectivity data.

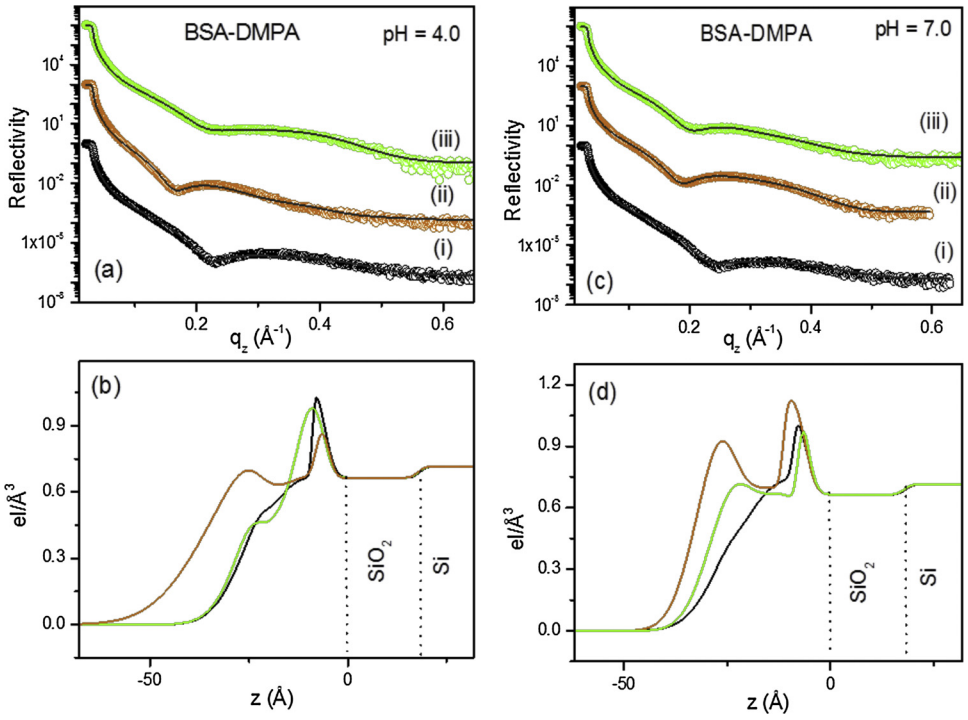

Fig. 7. X-ray reflectivity data (circle) and the corresponding fitted curves (solid line) obtained from the BSA-DMPA mixed films at (i) 10 mN/m and (ii) 40 mN/m during first compression, and again at (iii) 10 mN/m during second compression at (a) pH ≈ 4.0 and (c) pH ≈ 7.0. (b) and (d): corresponding electron density profiles extracted from the fitting of the reflectivity data.

structure is present also for D/B condition for both the pH values. For the films deposited at higher surface pressure, i.e., at pressure ≈40 mN/m, EDPs obtained shows that the film thickness and electron density are increased significantly indicating that the accumulation of the BSA molecules in both the hydrophobic tail part and hydrophilic headgroup regions of DMPA in combination with the compactness of the lipid molecules. Like B/D condition, here also the shifting of BSA molecules towards the lipid hydrophobic tail part is evidenced from the EDPs shown in Fig. 7(b) and (d) as relatively higher electron densities (≈0.58 and 0.78 el/Å^3) are obtained at ≈26 Å from the substrate surface in addition with the relatively higher electron densities (≈0.82 and 1.2 el/Å^3) near the substrate surface for pH ≈ 4.0 and 7.0 respectively. During the second compression and at the same lower pressure (π ≈ 10 mN/m), the EDPs show nearly the same or little less thickness as it was obtained during the first compression but the electron density is nearly the same or relatively higher for pH ≈ 4.0 and 7.0 respectively, which clearly suggests that the BSA molecules once lifted from the air-water interfaces finds difficulty in coming back to its initial state at pH ≈ 7.0, however, it is possible when the subphase pH is ≈4.0. Results obtained from EDPs thus clearly indicate that at pH ≈ 7.0 for both B/D and D/B conditions probably the strong hydrophobic interaction exists between the BSA and DMPA molecules due to which the shifted BSA molecules cannot come back from hydrophobic tail part of the lipids to the hydrophilic head part on the water surface.

From the insets of Fig. 1, which show compression-decompression cycles of B/D and D/B mixed films, it is evident that the hysteresis exists for both the pH but in case of pH ≈ 4.0 it was always less relative to pH ≈ 7.0 (Table 1) irrespective of any mixing ratio or mode of spreading of individual components (B/D or D/B). It is also visible that if the monolayer is allowed to compress further to a higher pressure (≈32 mN/m) and expand, it shows more hysteresis compared to the lower pressure (≈20 mN/m). As proteins such as BSA exhibits pH-dependent surface hydrophobicity, it is more likely to be hydrophobic at basic or neutral environment (pH ≈ 7.0) compared to an acidic environment (pH ≈ 4.0), where it demonstrates lesser surface hydrophobicity (Alizadeh-Pasdar and Li-Chan, 2000). Therefore, the mixed films formed by the BSA and DMPA at pH ≈ 4.0, i.e., when BSA holds a net positive charge and weak surface hydrophobicity, results in minor hysteresis compared to pH ≈ 7.0, when the surface hydrophobicity is stronger in BSA molecules. In addition, negatively charged headgroups of DMPA lipid may also have some effects on the DMPA-BSA interactions as BSA has net positive and negative surface charges at pH ≈ 4.0 and 7.0 respectively, however, in addition with the hydropbobic domains combination of both positive and negative local surface charge domains are also present on the protein surface. Thus, mostly on surface pressure and surface pH-dependent structural transformation occurs in the BSA and DMPA mixed films, but it is not dependent on B/D or D/B spreading conditions as shown as a cartoon in Fig. 8, i.e., a nearly similar effect is pronounced irrespective of spreading order that act as an advantage of using such film to study lipid-protein/protein-lipid model systems. Structural modification occurring above the isoelectric point of BSA is always higher than the one below the isoelectric point of BSA irrespective of the spreading order of the individual components. At higher pressure, as the area per molecule decreases, hydrophobic-hydrophobic interaction among the BSA and DMPA molecules enhances and hence more hysteresis was achieved for both the pH conditions. Thus, it can be concluded that in BSA-DMPA or DMPA-BSA mixed films, BSA molecules play an essential role in regulating the structural modification occurring during the compression-decompression cycles as BSA shows pH-dependent surface hydrophobicity. Besides, our results also confirm of having a better way of forming lipid-protein mixed model system, where the numbers of both the lipid and protein molecules can be controlled. In this study, the number of protein molecules was varied from 0 to 0.7355×10^{17}, whereas for lipid molecules it was varied from 0 to 1.358×10^{15}. Thus, BSA or most probably BSA-like protein molecules on the water surface can be used to form a lipid-protein mixed film in this better way. It will overcome the disadvantages of using proteins either by dissolving in or injecting through aqueous subphase as in such cases total number of protein molecules participating in the lipid-protein complex system is difficult to estimate.

4. Conclusions

Studies on lipid (DMPA) and protein (BSA) mixed films are done by varying the ratio of protein and lipid, and also by altering the order of molecules spread at the air-water interface for two different pH

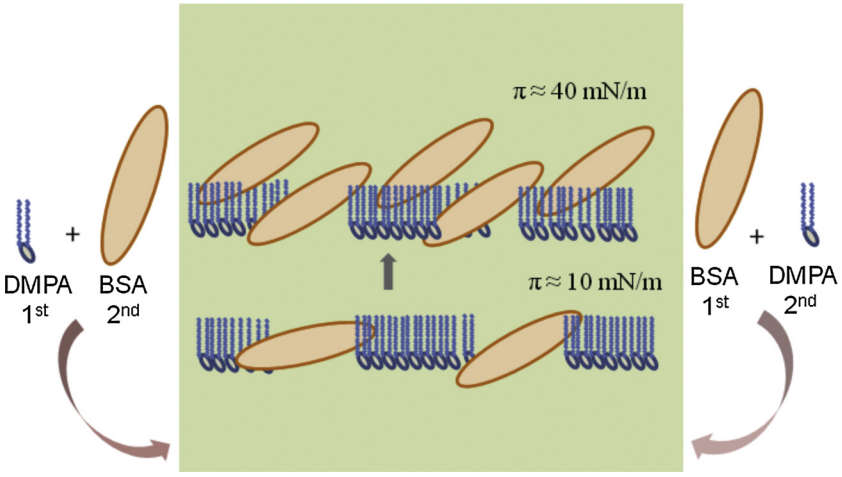

Fig. 8. Schematic representation of the structural modifications of the protein-lipid mixed films for lower (10 mN/m) and higher (40 mN/m) surface pressure at a particular subphase pH for two different spreading conditions, i.e., for B/D and D/B conditions. Nearly the same structural and morphological information are obtained for both the BSA-DMPA and DMPA-BSA mixed film.

conditions (pH ≈ 4.0 and 7.0), i.e., below and above the isoelectric point of BSA. The nearly reversible π–*A* isotherm cycles obtained from the pure BSA monolayer confirms that desorption of BSA into the water subphase is negligible. Compression-decompression π–*A* isotherm cycles obtained from the protein-lipid mixed films show similar results irrespective of the spreading order of the individual components. At pH ≈ 4.0, when BSA molecules are positively charged and weakly hydrophobic always shows less hysteresis compared to pH ≈ 7.0, when BSA molecules are relatively more hydrophobic. For both the pH conditions, compression-decompression isotherm cycles conducted up to higher surface pressure show more hysteresis compared to their lower pressure counterparts, which indicates that as more hydrophobic portions interact with each other, the relatively higher structural modification occurs as BSA molecules moves toward the hydrophobic tail portion of lipid (DMPA) monolayer. X-ray scattering study on protein-lipid thin film shows that with the barrier compression BSA molecules get shifted from hydrophilic head part to the more hydrophobic tail part of the lipids for both the pH conditions. The results are consistent irrespective of the spreading order of BSA/DMPA molecules as nearly the same structural and morphological information is obtained for both the conditions, i.e., for BSA-DMPA and DMPA-BSA mixed films. Thus, the method used in this work can be considered as suitable to study the protein-lipid 2D systems using the BSA protein molecule.

Declaration of Competing Interest

None.

Acknowledgments

The work is supported by Department of Science and Technology (DST), Nano Mission, India (Grant No. SR/NM/NS-1035/2013(G)). Authors also acknowledge Council for Scientific and Industrial Research (CSIR), Govt. of India for CSIR-SRF fellowship (Grant No: 09/835(0027)/2019-EMR-I).

References

Abney, J.R., Owicki, J.C., 1985. Theories of protein-lipid and protein-protein interactions in membranes. In: Watts, A., de Pont, J.J.H.H.M. (Eds.), Progress in Protein-Lipid Interactions. Elsevier Science Publisher, Amsterdam, pp. 1–60.
Alizadeh-Pasdar, N., Li-Chan, E.C.Y., 2000. J. Agric. Food Chem. 48, 328–334.
Basu, J.K., Sanyal, M.K., 2002. Phys. Rep. 363, 1–84.
Bunker, B.C., Rieke, P.C., Tarasevich, B.J., Campbell, A.A., Fryxell, G.E., Graff, G.L., Song, L., Liu, J., Virden, J.W., McVay, G.L., 1994. Science 264, 48–55.
Caetano, W., Ferreira, M., Tabak, M., Sanchez, M.I.M., Oliveira, O.N., Kruger, P., Schalke, M., Losche, M., 2001. Biophys. Chem. 91, 21–35.
Castlden, J.A., 1969. J. Pharmacol. Sci. 58, 149–165.
Chou, T.-H., Chang, C.-H., 2000. Colloids Surf. B: Biointerfaces 17, 71–79.
Cremer, P.S., Boxer, S.G., 1999. J. Phys. Chem. B 103, 2554–2559.
Daillant, J., Gibaud, A., 2009. X-Ray and Neutron Reflectivity: Principles and Applications. Springer, Berlin.
Das, K., Sah, B.K., Kundu, S., 2017. Phys. Rev. E 95 022804-1- 022804-8.
de Souza, N.C., Caetano, W., Itri, R., Rodrigues, C.A., Oliveira, O.N., Giacometti, J.A., Ferreira, M., 2006. J. Colloid Interface Sci. 297, 546–553.
Douglas, K., 1996. In: Mann, S. (Ed.), Biomimetic Materials Chemistry. VCH Publishers Inc., New York.
Fidelio, G.D., Maggio, B., Cumar, F.A., 1984. Chem. Phys. Lipids 35, 231–245.
Gaines, G.L., 1966. Insoluble Monolayers at Liquid-gas Interfaces. Interscience Publishers.
Garcia-Manyes, S., Oncins, G., Sanz, F., 2006. Electrochim. Acta 51, 5029–5036.
Giacomelli, C.E., Norde, W., 2001. J. Colloid Interface Sci. 233, 234–240.
Grainger, D.W., Ahlers, M., Reichert, A., Ringsdorf, H., Salesse, C., Herron, J.N., Lim, K., 1992. J. Control. Release 19, 201–218.
Horcas, I., Fernández, R., Gómez-Rodríguez, J.M., Colchero, J., Gómez-Herrero, J., Baro, A.M., 2007. Rev. Sci. Instrum. 78 013705-1-013705-8.
Jahnig, F., Vogel, H., Best, L., 1982. Biochemistry 21, 6790–6798.
Keller, C.A., Kasemo, B., 1998. Biophys. J. 75, 1397–1402.
Kondo, A., Oku, S., Higashitani, K., 1991. J. Colloid Interface Sci. 143, 214–221.
Kong, J., Yu, S., 2007. Acta Biochim. Biophys. Sin. 39, 549–559.
Kundu, S., Das, K., Aswal, V.K., 2013. Chem. Phys. Lett. 578, 115–119.
Kundu, S., Datta, A., Sanyal, M.K., Daillant, J., Luzet, D., Blot, C., Struth, B., 2006. Phys. Rev. E 73 061602-1-061602-6.
Kundu, S., Datta, A., Hazra, S., 2005. Langmuir 21, 5894–5900.
Laukkanen, M.-L., Alfthan, K., Keinänen, K., 1994. Biochemistry 33, 11664–11670.
Li, J.B., Zhao, J., Wu, J., Miller, R., 1998. Nahrung 42, 232–233.
Lösche, M., Mohwaid, M., 1984. Eur. Biophys. J. 11, 35–42.
Martin, M.T., Prieto, I., Camacho, L., Mobius, D., 1996. Langmuir 12, 6554–6560.
Mayor, M., Hagfeldt, A., Grätzel, M., Walder, L., 1996. Chimia 50, 47–49.
McConnell, H.M., De Koker, R., 1992. J. Phys. Chem. 96, 7101–7103.
McConnell, H.M., Moy, V.T., 1988. J. Phys. Chem. 92, 4520–4525.
Muramatsu, M., Sobotka, H., 1962. J. Phys. Chem. 66, 1918–1923.
Murayama, K., Tomida, M., 2004. Biochemistry 43, 11526–11532.
Norde, W., Favier, J.P., 1992. Colloids Surf. 64, 87–93.
Okahata, O., Tsuruta, T., Ijiro, K., Ariga, K., 1989. Thin Solid Films 180, 65–72.
Parratt, L.G., 1954. Phys. Rev. 95, 359–369.
Peppas, N., Langer, R., 1994. Science 263, 1715–1720.
Peters, T., 1985. Adv. Protein Chem. 37, 161–245.
Reimhult, E., Hook, F., Kasemo, B., 2003. Langmuir 19, 1681–1691.
Sackmann, E., 1984. Physical basis of trigger processes and membrane structures. In: Chapmann, D. (Ed.), Biological Membranes. Academic Press, New York, pp. 105–143.
Sah, B.K., Kundu, S., 2017. Colloid Surf. B: Biointerfaces 159, 696–704.
Sasaki, D.Y., Shnek, D.R., Pack, D.W., Arnold, F.H., 1995. Angew. Chem. Int. Ed. Engl. 34, 905–907.
Schalke, M., Krüger, P., Weygand, M., Lösche, M., 2000. Biochim. Biophys. Acta 1464, 113–126.
Stallberg-Stenhagen, S., Stenhagen, E., 1945. Nature 156, 239–240.
Stelzle, M., Weissmueller, G., Sackmann, E., 1993. J. Phys. Chem. 97, 2974–2981.
Tolan, M., 1999. X-Ray Scattering From Soft matter Thin Films. Springer, Berlin.
Tronin, A., Dubrovsky, T., De Nitti, C., Gussoni, A., Erokhin, V., Nicolini, C., 1994. Thin Solid Films 238, 127–132.
Vaknin, D., Krüger, P., Lösche, M., 2003. Phys. Rev. Lett. 90 178102-1–178102-4.
Vernoux, N., Maniti, O., Besson, F., Granjon, T., Marcillat, O., Vial, C., 2007. J. Colloid Interface Sci. 310, 436–445.
Wang, X.L., He, Q., Zheng, S.P., Brezesinski, G., Mohwald, H., Li, J.B., 2004. J. Phys. Chem. B 108, 14171–14177.
Wang, X., Zhang, H., Cui, G., Li, J.B., 2001. J. Mol. Liq. 90, 149–156.
Wang, X., Zhang, H., Wu, J., Cui, G., Li, J.B., Brezesinski, G., 2002. Colloid Surf. B: Biointerfaces 23, 339–347.
Whitesides, G.M., Boncheva, M., 2002. Proc. Natl. Acad. Sci. U. S. A. 99, 4769–4774.
Zhang, H., Wang, X., Cui, G., Li, J.B., 2000. Colloid Surf. A: Physicochem. Eng. Asp. 175, 77–82.
Zhu, D.G., Petty, M.C., Ancelin, H.H., Yarwood, J., 1989. Thin Solid Films 176, 151–156.